Anal Bioanal Chem
DOI 10.1007/s00216-013-7135-3

RESEARCH PAPER

Micro- to nanostructured poly(pyrrole-nitrilotriacetic acid) films via nanosphere templates: applications to 3D enzyme attachment by affinity interactions

Andreea Cernat · Alan Le Goff · Michael Holzinger · Robert Sandulescu · Serge Cosnier

Received: 7 April 2013 / Revised: 6 June 2013 / Accepted: 10 June 2013

Abstract We report the combination of latex nanosphere lithography with electropolymerization of N-substituted pyrrole monomer bearing a nitrilotriacetic acid (NTA) moiety for the template-assisted nanostructuration of poly(pyrrole-NTA) films and their application for biomolecule immobilization. The electrodes were modified by casting latex beads (100 or 900 nm in diameter) on their surface followed by electropolymerization of the pyrrole-NTA monomer and the subsequent chelation of Cu^{2+} ions. The dissolution of the nanobeads leads then to a nanostructured polymer film with increased surface. Thanks to the versatile affinity interactions between the (NTA)Cu^{2+} complex and histidine- or biotin-tagged proteins, both tyrosinase and glucose oxidase were immobilized on the modified electrode. Nanostructuration of the polypyrrole via nanosphere lithography (NSL) using 900- and 100-nm latex beads allows an increase in surface concentration of enzymes anchored on the functionalized polypyrrole electrode. The nanostructured enzyme electrodes were characterized by fluorescence microscopy, 3D laser scanning confocal microscopy, and scanning electron microscopy. Electrochemical studies demonstrate the increase in the amount of immobilized biomolecules and associated biosensor performances when achieving NSL compared to conventional polymer formation without bead template. In addition, the decrease in nanobead diameter from 900 to 100 nm provides an enhancement in biosensor performance. Between biosensors based on films polymerized without nanobeads and with 100-nm nanobeads, maximum current density values increase from 4 to 56 μA cm^{-2} and from 7 to 45 μA cm^{-2} for biosensors based on tyrosinase and glucose oxidase, respectively.

Keywords Nanosphere lithography · Polypyrrole · Biosensor · Affinity binding · Tyrosinase · Glucose oxidase

Introduction

Electrochemical enzymatic biosensors rely on immobilization strategies that maintain the biological activity of the immobilized enzyme while ensuring good accessibility. We and others have developed affinity interactions for the rapid and soft immobilization of bioreceptors on electrodes [1–3]. In particular, we and others have shown the great ability of electrogenerated polymers to achieve stable and reproducible modification of electrode surfaces [4–6]. By functionalizing monomers with an affinity partner, a wide range of bioreceptors such as enzymes, antibodies, DNA, RNA, or aptamers can elegantly be immobilized via specific supramolecular interactions such as biotin/avidin/biotin [7], phosphonate/Mg^{2+}/phosphate [8], and adamantane/ß-cyclodextrin [9]. In this context, we recently developed a versatile electropolymerized affinity system based on the noncovalent immobilization of histidine- and biotin-tagged biomolecules on a poly(pyrrole-nitrilotriacetic acid) film (poly-(pyrrole-NTA)). Chelation of Cu^{2+} by the polymerized NTA group allows the coordination of histidine and biotin tags and hence the immobilization of a wide range of tagged biomolecules such as proteins [10, 11] or oligonucleotides [8, 12]. In terms of nanostructuration of electrogenerated polymers for biosensing applications, carbon nanotubes represent one of the most efficient templates to form highly porous nanostructured polymers that allow the immobilization of a high amount of bioreceptor units and optimal diffusion of the analytes and substrates [13–15]. We also demonstrated the facile functionalization of carbon nanotube electrodes with

Published in the special issue *Analytical Science in France* with guest editors Christian Rolando and Philippe Garrigues.

A. Cernat · R. Sandulescu
Analytical Chemistry Department, Faculty of Pharmacy, Iuliu Haţieganu University of Medicine and Pharmacy, Pasteur st. 4, 400349 Cluj-Napoca, Romania

A. Le Goff · M. Holzinger · S. Cosnier (✉)
Département de Chimie Moléculaire UMR-5250, ICMG FR-2607, CNRS Université Joseph Fourier, BP-53, 38041 Grenoble, France
e-mail: serge.cosnier@ujf-grenoble.fr

Published online: 21 June 2013

N-substituted polypyrrole films [16–18]. This constitutes an indirect method to obtain nanostructured polymers by surrounding the carbon nanotube matrix and hence to enhance the enzyme surface concentration and the diffusion of substrates.

Nanosphere lithography (NSL) using latex or silica beads has been widely employed to control the nano-and microstructruration of materials such as metals [19–21] or conducting polymers [22–25]. These beads form ordered and closely packed templates that can easily be removed by simple dissolution in organic solvents leaving a porous surface with controlled nanostructure, thus possessing a high specific surface. Here, we show the combination of NSL with electropolymerization of a pyrrole monomer bearing a NTA group to demonstrate the possible use of NSL to achieve immobilization of high amounts of enzymes and, by consequence, to enhance electrochemical biosensing performances. This putative enhancement brought by these nanostructured polypyrrole-NTA surfaces was studied via the immobilization of two biomolecule models using biotin-labeled tyrosinase and histidine-tagged glucose oxidase. The biosensing performances of the respective enzyme electrodes were investigated towards the detection of glucose and catechol, respectively.

Experimental

Chemicals and materials

FITC-labeled avidin, Na_2HPO_4, NaH_2PO_4, catechol, glucose oxidase (GOx), and polyphenol oxidase were provided from Sigma. $AgNO_3$, glucose, hydroquinone, and $CuCl_2$ were purchased from Prolabo (VWR International), $LiClO_4$ from Fluka, and EZ-link Sulfo-NHS-LC-biotin from Pierce. 3′-BiotinTEG CPG was purchased from Glen Research Corporation. Acetonitrile (Rathburn, HPLC grade) and lithium perchlorate were used as received. Ultrapure water (18.2 Ω cm) was used for all aqueous solutions. All chemicals were of analytical grade and used as received. Solutions of glucose were allowed to mutarotate for 1 day and were kept refrigerated. 11-Pyrrol-1-*yl*-undecanoic acid N_α,N_α-bis(carboxymethyl)-L-lysine amide (pyrrole-NTA) was synthesized according to a reported procedure [10].

Histidine-tagged glucose oxidase was synthesized as follows: to 5 mL of a 0.1 mol L^{-1} phosphate buffer (pH=6), 6.07 mg (*S*)-2-amino-3-(4-imidazolyl)propionic acid (L-histidine, 39.1 μmol) and 5.08 mg 1-ethyl-3-(3-dimethylaminopropyl)carbodiimide hydrochloride (26.5 μmol) were dispersed in an ultrasound bath. To this solution, 5.148 mg glucose oxidase was added. The reaction mixture was vigorously stirred for 24 h at 4 °C. Modified glucose oxidase was purified by centrifugation (30000 MWCO concentrator with PES membrane at 6,000 G) at 4 °C. The resulting enzyme concentrations were quantified using UV spectroscopy by measuring the intensity of a 280-nm band (yield ≈40 %, each). Its activity, determined using amperometry, is 150 U mg^{-1}. Tyrosinase (5 mg, 39 nmol) was biotinylated with sulfo-NHS-LC-biotin (78 μL, 10^{-2} mol L^{-1}, 780 nmol) in 5 mL phosphate buffer (pH=6, 0.1 mol L^{-1}) for 2 h at 4 °C. Modified enzymes were purified by centrifugation (30000 MWCO concentrator with PES membrane at 6,000 G) at 4 °C.

Electrochemical instrumentation

All electrochemical studies were performed with a conventional three-electrode system. A Ag/AgCl reference and a saturated calomel electrode (SCE) were used for electropolymerization and biosensing experiments, respectively. A Pt wire electrode was used as counter electrode. The working electrodes were platinum (5 mm diameter) and glassy carbon (3 mm diameter), both polished with 2 μm diamond paste followed by rinsing with distilled water and ethanol. The electropolymerization experiments were conducted on an Autolab PGstat100 potentiostat. The amperometric measurements were carried out with a Tacussel PRG-DL potentiostat.

Elaboration of enzyme electrodes and characterization

The template was created on working electrodes by drop casting of a 0.5-wt% ethanol suspension of latex spheres 900 nm (5 μl) and 100 nm (3×5 μl) in diameter and allowed to dry at room temperature for 10–30 min. After the formation of poly(pyrrole-NTA) film by scanning the potential repeatedly (ten scans) from 0 to 0.85 V vs Ag/AgCl at 0.1 V s^{-1} in a 10 mM pyrrole-NTA MeCN solution in 0.1 M TBAP, the resulting electrodes were immersed for 15–20 h in tetrahydrofuran (THF) in order to remove the latex template. The electrodes were rinsed with ethanol and distilled water. The resulting electrodes were soaked for 30 min in 10 mM $CuCl_2$ acetate buffer solution (0.1 M, pH=4.8). The modified electrodes were then successively washed with 0.5 M NaCl and phosphate buffer. The immobilization of tagged enzymes on the modified electrode was performed by incubation in the respective solutions containing the tagged enzymes (0.5 mg mL^{-1} for biotin-tagged tyrosinase and 0.5 mg mL^{-1} for histidine-tagged GOx) and kept at 4 °C for 1–2 h. The resulting electrodes were washed in stirred phosphate buffer for 5–10 min. The morphology of the modified electrodes was investigated by SEM using an ULTRA 55 field emission scanning electron microscopy (FESEM) based on the Gemini FESEM column with beam booster (Nanotechnology Systems Division, Carl Zeiss NTS GmbH, Germany) and tungsten gun or by a Keyence 3D laser scanning microscope. Fluorescence microscopic images were recorded with an Olympus BX61 microscope (exciter: D350/50, emitter: D470/40, beam splitter: 400dclp; Japan).

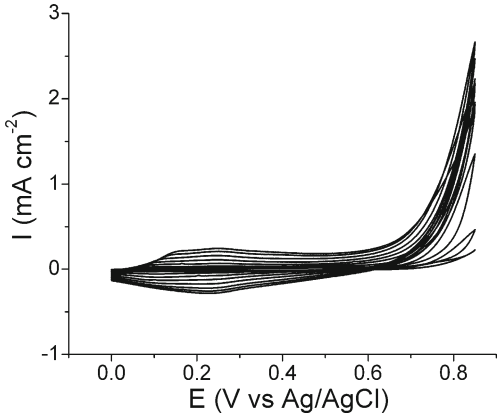

Fig. 1 Cyclic voltammograms (ten scans) in MeCN–TBAP (0.1 M) containing 10 mM of pyrrole-NTA monomer on GC electrode functionalized with 100-nm-diameter nanospheres. v=0.1 V s^{-1}

Results and discussion

Nanostructured enzyme electrodes were prepared in five successive steps. After the deposition of latex beads on Pt or GC electrodes, pyrrole-NTA was electropolymerized onto the nanobeads. The latter form a highly ordered network at the surface of the electrodes. Figure 1 shows the successive cyclic voltammograms corresponding to the typical polymerization of pyrrole-NTA in the presence of 100-nm-diameter nanobeads. It is noteworthy that the oxidative scanning is stopped at the foot of the irreversible oxidation of pyrrole to avoid overoxidation of the polypyrrolic chain and hence the loss of the polymer conductivity.

The electrodeposition of poly(pyrrole-NTA) is confirmed by the appearance and increase of a reversible peak system at 0.2 V corresponding to the well-known electroactivity of the steadily growing polypyrrole backbone for each scan. After dissolution of the latex nanobeads in THF, the surface morphology of the electrogenerated polymer was characterized by laser scanning microscopy when the 900-nm-diameter nanobeads were used and SEM when the 100-nm-diameter nanobeads were casted on the surface.

Figure 2A shows the 3D image obtained for the nanostructured surface using 900-nm-diameter spheres as templates. The formation of the polymer surrounding the beads is confirmed by the well-ordered pores formed after the dissolution step, leading to a controlled microstructure of the N-substituted polypyrrole, especially for 900-nm beads. In this case, the electrogeneration of the poly(pyrrole-NTA) was optimized to obtain a 350 (±50)-nm-thick film surrounding the 900-nm spheres. The dissolution of the beads creates well-defined 900-nm-diameter pores with approximately 350 (±50)-nm depth. For the 100-nm nanospheres, SEM was employed to characterize the surface pattern of the polymer. Panels b and c of Fig. 2 show the highly porous and well-ordered matrix obtained after dissolution of the 100-nm nanospheres. In contrast to the easy deposition of a regular and compact monolayer of 900-nm nanobeads, the use of the 100-nm nanobeads leads to the formation of several layers on the electrode surface. This is corroborated by the thickness of the polymer which is approximately between 200 and 300 nm. Consequently, after electrodeposition of the polymer and nanobead dissolution, the electrogenerated polypyrrole exhibits cheese-like multilayer porosity. The nanostructured films are stable for at least 2 weeks under storage at ambient temperature and exposed to air.

The biosensor setup was finally completed via incubation of the nanostructured electrode in a 10-mM $CuCl_2$ solution followed by incubation in the tagged enzyme solution. We employed two enzymes as biomolecule model, tyrosinase and GOx, respectively tagged with two types of affinity partners, biotin and histidine. With the aim to demonstrate the specific anchoring of protein onto the nanostructured polymer, we investigated the immobilization of enzymes by fluorescence microscopy. After electrodeposition of pyrrole-NTA on 900-nm latex spheres and dissolution of the latter, the modified electrodes were successively incubated with Cu^{2+} solution, a biotinylated tyrosinase solution, and finally with a fluorescent avidin (FITC-labeled avidin) solution. The modified electrodes were vigorously washed after each step. Figure 3 shows the fluorescence images of the enzyme electrode. It appears that the fluorescence phenomenon is homogenously localized

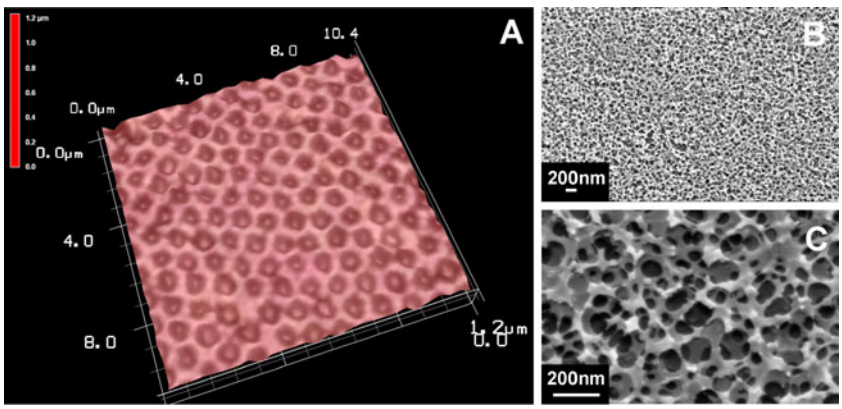

Fig. 2 **A** Confocal 3D microscope image of an electrode functionalized with poly(pyrrole-NTA) electrogenerated on 900-nm beads. **B**, **C** SEM image of an electrode functionalized with poly(pyrrole-NTA) electrogenerated on 100-nm beads

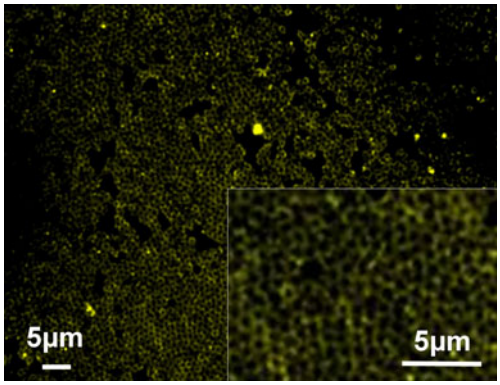

Fig. 3 Fluorescence microscope images of an electrode modified with a biotinylated tyrosinase followed by incubation with FITC-labeled avidin. The electrode was previously functionalized with poly(pyrrole-NTA)/Cu^{2+} electrogenerated on 900-nm beads that were dissolved after the polymer formation. The control experiment was performed with nontagged enzymes and exhibited negligible fluorescence

on the microstructured polymer (Fig. 3 inset). This indicates that the fluorescent avidin was bound by affinity interactions to the biotinylated enzyme, the latter acting as a bridge between the polymer and avidin. Control experiments were carried out with a microstructured polymer successively incubated with regular glucose oxidase and tyrosinase and FITC-labeled avidin. The absence of fluorescence on the resulting modified electrode reflects the lack of nonspecific adsorption of FITC-labeled avidin on the polymer. This corroborates thus the specific binding of biotinylated tyrosinase by coordination of the biotin residues on the Cu^{2+}-NTA groups at the nanostructured surface of the modified electrode.

In the presence of oxygen, tyrosinase catalyzes the oxidation of phenols and *o*-diphenols such as catechol to *o*-quinones allowing an electrochemical detection of the enzyme substrate by reduction (Eq. 1).

$$\text{catechol} + \tfrac{1}{2}\,O_2 = \text{benzoquinone} + H_2O \qquad (1)$$

When the enzyme electrode is poised at −0.2 V vs SCE, the enzymatically generated quinone is electrochemically reduced into catechol at the underlying surface of the glassy carbon electrode. The regenerated substrate can then be reoxidized by the enzyme, leading to an amplified biosensor response [26, 27, 24–26]. The reduction of *o*-quinone formed by oxidation of catechol at our tyrosinase-modified electrode was therefore investigated. Figure 4 presents the calibration curves for catechol recorded at modified electrodes elaborated without nanobeads and using 900- and 100-nm latex beads.

The calibration curves were quasilinear with low catechol concentrations and then curved gradually at higher concentrations, a pseudo plateau being reached reflecting the saturation of the immobilized enzymes. The shape of these curves corresponds to a Michaelis–Menten kinetic for the electrochemical activity of the immobilized enzymes. These characteristics are summarized in Table 1. Expectedly, percentages of errors are increased by the nanosphere lithography step. This is likely caused by inhomogeneity during the formation of the controlled porosity during the bead dissolution process.

The apparent Michaelis–Menten constant (K_M^{app}), which reflects the enzyme–substrate affinity and the microenvironment of the enzyme, is similar for the three modified electrodes, i.e., 0.11 and 0.12 mM. This indicates a similar environment for the enzyme immobilized on the poly(pyrrole-NTA) electrodes as well as similar steric hindrances for the permeation and electrochemical detection of the generated quinone. Nevertheless, it appears that the biosensor performances in terms of sensitivity and limit of detection (LOD) are clearly better for biosensors based on nanostructured films than those recorded for biosensor based on polypyrrole formed without template (Table 1).

In addition, the maximum current density (I_{max}) values obtained for nanostructured polymers generated using 900- and 100-nm nanobeads are, respectively, 6 times and 14 times higher compared to conventional poly(pyrrole-NTA) film. Taking into account that the I_{max} value is directly proportional to the enzyme loading, these results confirm that a higher amount of enzymes was immobilized thanks

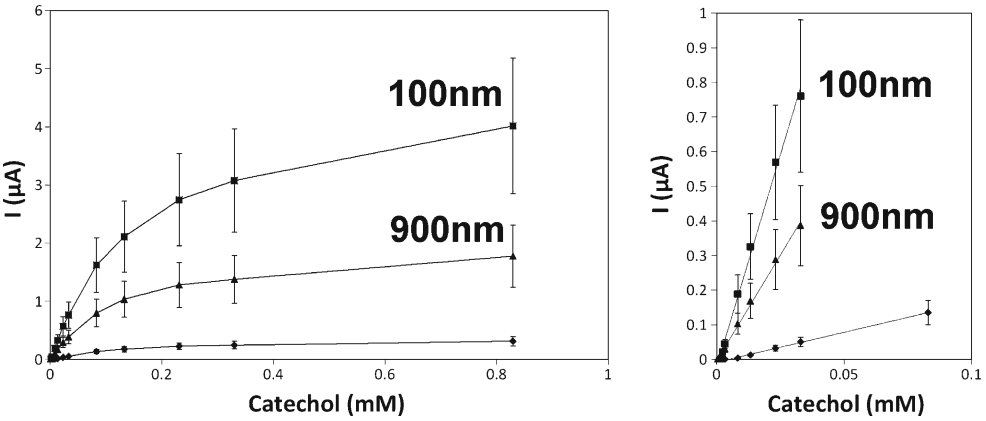

Fig. 4 Calibration curves for catechol at GC electrodes functionalized with poly(pyrrole-NTA) and successively incubated with $CuCl_2$ (10 mM) and biotin-tagged tyrosinase: (*diamonds*) in the absence of nanobeads, (*triangles*) with 900-nm-diameter beads, and (*squares*) with 100-nm nanobeads; (*right*) plot of the linear part. (Measurements performed by chronoamperometry at E=−0.2 V vs SCE, 0.1 M PBS, pH 7, 25 °C)

Table 1 Glucose and catechol biosensing performances for micro- to nanostructured poly(pyrrole-NTA) electrodes

	Latex sphere diameter (nm)	K_M^{app} (mM)	I_{max} (μA cm^{-2})	Sensitivity (mA mol^{-1} L cm^{-2})	LOD (μM)
Catechol oxidation by tyrosinase	None	0.12	4.3 (±1.1)	24 (±6)	4.8 (±1.2)
	900	0.11	25 (±8)	171 (±51)	0.38 (±0.11)
	100	0.11	56 (±16)	344 (±99)	0.98 (±0.28)
Glucose oxidation by GOx	None	12	7.3 (±1.4)	0.50 (±0.10	77 (±15)
	900	10	12 (±3)	1.0 (±0.2)	28 (±6)
	100	10	45 (±9)	3.9 (±1.1)	19 (±6)

to the 100-nm nanobead template, leading to a more than one order of magnitude enhancement of biosensor performance. Nevertheless, these performances remain inferior to those reported for catechol biosensors based on enzyme entrapment [28]. For instance, the entrapment of tyrosinase within Fe_3O_4-chitosan nanocomposites or mesoporous silica leads to higher catechol sensitivity (7.71 and 45 A mol^{-1} L cm^{-2}, respectively) and a more sensitive detection limit, namely 25 nmol L^{-1} for Fe_3O_4-chitosan and 0.78 nmol L^{-1} for silica [29, 30]. However, it should be noted that the amount of entrapped enzyme largely exceeds the amount corresponding to coverage by a simple enzyme monolayer, highlighting the importance of this parameter on the performance of enzyme electrodes. Indeed, the entrapped amount of tyrosinase in mesoporous silica (270 μg cm^{-2}) and Fe_3O_4–chitosan composite (480 μg cm^{-2}) are equivalent to 545 and 970 compact enzyme layers [31].

Similarly to the immobilization of biotinylated tyrosinase, we investigated the affinity binding of GOx tagged with histidine groups. Histidine can easily be attached to the poly(pyrrole-NTA)/Cu^{2+} moiety via affinity interactions with the chelated Cu^{2+} sites. Since GOx catalyzes the glucose oxidation with the concomitant O_2 reduction forming H_2O_2, its activity can be monitored through the electrochemical oxidation of H_2O_2. With the aim to estimate the electroenzymatic activity of the immobilized GOx, the biosensor response to glucose concentration was recorded.

The enzyme electrodes were thus maintained at a potential of 0.6 V in 0.1 M PBS (pH 7, 25 °C) to detect H_2O_2 at the underlying Pt surface. Figure 5 shows the amperometric signal corresponding to the electrochemical oxidation of the enzymatically produced H_2O_2 as a function of glucose concentration.

As observed for immobilization of tyrosinase, the three modified electrodes exhibit a Michaelis–Menten behavior that characterizes the immobilization of GOx. A K_M^{APP} value of about 10 mM was determined for all electrodes indicating that the enzyme microenvironment is similar for the three electrode configurations. It is noteworthy that the K_M^{app} value is in good agreement with those of glucose biosensors and far below the K_M (33 mM) of GOx in solution. This difference may be ascribed to a depletion of oxygen within the enzyme layer. Table 1 summarizes the performances of the three enzyme electrodes for the determination of glucose.

Compared to the control poly(pyrrole-NTA) film, the use of nanobead templates leads to enzyme electrodes exhibiting higher glucose sensitivity and lower detection limits, the best performance being recorded with 100-nm nanobead template. The latter provides an eightfold increase in the glucose

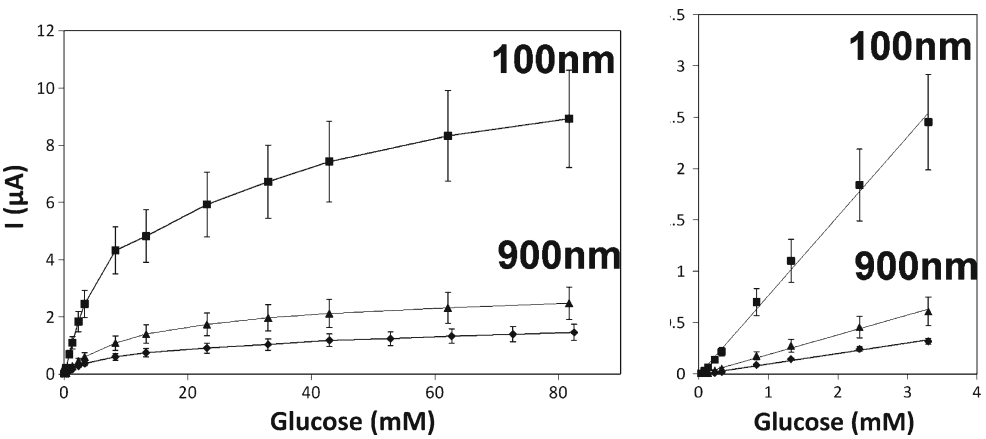

Fig. 5 Calibration curves for glucose at Pt electrodes functionalized with poly(pyrrole-NTA) and successively incubated with $CuCl_2$ (10 mM) and histidine-tagged GOx: (*diamonds*) in the absence of nanobeads, (*triangles*) with 900-nm-diameter beads, and (*squares*) with 100-nm nanobeads; (*right*) plot of the linear part. (Measurements performed by chronoamperometry at E=0.6 V vs SCE, 0.1 M PBS, pH 7, 25 °C)

sensitivity whereas only a two fold increase was observed for the 900-nm nanobeads. As demonstrated with tyrosinase electrodes, the use of 100-nm nanobeads leads to a biosensor exhibiting the highest I_{max} value, namely 45 μA cm^{-2}. Compared to the I_{max} value (7 μA cm^{-2}) observed for regular poly(pyrrole-NTA) film, the enhancement of enzyme loading seems to be equivalent to the formation of six compact enzyme monolayers. This drastic improvement in the amount of immobilized enzyme was corroborated by the comparison of the I_{max} values (3.4–11.5 μA cm^{-2}) previously reported for the anchoring of one monolayer of histidine-tagged GOx onto poly(pyrrole-NTA) films [10, 11]. These analytical performances were also compared with those reported for electrodes composed of four monolayers of biotin-tagged GOx or five compact layers of biotin-tagged tyrosinase attached by avidin–biotin interactions on a biotinylated polypyrrole film [31, 32]. The corresponding I_{max} values, 4 and 51.29 μA cm^{-2} for glucose and catechol, respectively, corroborate the improvement in enzyme immobilization brought by the use of the 100-nm nanobead template. These results also illustrate the advantage of the affinity system based on histidine and biotin coordination onto poly(pyrrole-NTA)-Cu^{2+}film compared to avidin–biotin interactions with biotinylated polypyrrole films. This may be ascribed to a better polymer permeability towards the diffusion of enzyme product to be detected at the electrode surface and the absence of avidin as intermediary bridge between the protein and the film. In the same vein as tyrosinase electrodes, higher performances in terms of sensitivity and detection limits were reported for glucose biosensors based on the entrapment or coprecipitation of high GOx amounts (200–2,500 μg cm^{-2}) in matrices like clay nanoparticles, organic gels, multiwalled carbon nanotube (MWCNT) deposits, MWCNT–chitosan–nano ZnO composites, or polymers [28, 33–35]. Nevertheless, it should be noted that the sensitivity value is similar to that recently described for the covalent binding of GOx onto a 3D matrix of carbon nanotubes, namely 4.05 A mol^{-1} L cm^{-2} [36].

In conclusion, this work shows the well-defined control over micro- to nanostructuration of N-substituted polypyrrole films and the induced increase in a specific polymer surface for immobilization of proteins. The investigation of the surface morphologies using microscopic methods underlines the efficient homogenous nanosphere lithography via electrogeneration poly(pyrrole-NTA) around nanobead layers of different sizes. Such shaped polymer serves as a versatile platform for the immobilization of two model enzymes with different tags, showing the highest biosensing performances for the smallest nanosphere sizes used as template. Taking into account the large molecular weight of these proteins (128,000–189,000), the facile immobilization of several equivalent monolayers of biomolecules via affinity interactions underlines the excellent accessibility to the nanostructured polymer surface. The combination of NSL with electrogenerated affinity polymers thus represents a promising avenue for future developments of enzyme electrodes and electrochemical immunosensors and DNA sensors.

Acknowledgments The authors are grateful for the financial support to POS-DRU 88/1.5/S/56949 UMF Iuliu Hatieganu research grant (27027/3/15.11.2011) and PN II IDEI grant 338/2011. The authors also thank the ANR Investissements d'avenir-Nanobiotechnologies 10-IANN-0-02 programs and the platform "Functionalization of Surfaces and Transduction" of the scientific structure "Nanobio" for providing facilities and partial financial support.

References

1. Cosnier S (2007) Recent advances in biological sensors based on electrogenerated polymers: a review. Anal Lett 40:1260–1279
2. Cosnier S (2005) Affinity biosensors based on electropolymerized films, affinity biosensors based on electropolymerized films. Electroanal Electroanal 17(17:1701):1701–1715, 1715
3. Ronkainen NJ, Halsall HB, Heineman WR (2010) Electrochemical biosensors. Chem Soc Rev 39:1747
4. Cosnier S, Holzinger M (2011) Electrosynthesized polymers for biosensing. Chem Soc Rev 40:2146–2156
5. Dhand C, Das M, Datta M, Malhotra BD (2011) Recent advances in polyaniline based biosensors. Biosens Bioelectron 26:2811–2821
6. Zanardi C, Terzi F, Seeber R (2012) Polythiophenes and polythiophene-based composites in amperometric sensing. Anal Bioanal Chem 405:509–531
7. Cosnier S, Lepellec A (1999) Poly(pyrrole–biotin): a new polymer for biomolecule grafting on electrode surfaces. Electrochim Acta 44:1833–1836
8. Baur J, Gondran C, Holzinger M et al (2010) Label-free femtomolar detection of target DNA by impedimetric DNA sensor based on poly(pyrrole-nitrilotriacetic acid) film. Anal Chem 82:1066–1072
9. Holzinger M, Bouffier L, Villalonga R, Cosnier S (2009) Adamantane/β-cyclodextrin affinity biosensors based on single-walled carbon nanotubes. Biosens Bioelectron 24:1128–1134
10. Haddour N, Cosnier S, Gondran C (2005) Electrogeneration of a poly(pyrrole)-NTA chelator film for a reversible oriented immobilization of histidine-tagged proteins. J Am Chem Soc 127:5752–5753
11. Baur J, Holzinger M, Gondran C, Cosnier S (2010) Immobilization of biotinylated biomolecules onto electropolymerized poly(pyrrole-nitrilotriacetic acid)–Cu^{2+} film. Electrochem Commun 12:1287–1290
12. Wenjuan Y, Le Goff A, Spinelli N et al (2013) Electrogenerated trisbipyridyl Ru(II)-/nitrilotriacetic-polypyrene copolymer for the easy fabrication of label-free photoelectrochemical immunosensor and aptasensor: application to the determination of thrombin and anti-cholera toxin antibody. Biosens Bioelectron 42:556–562
13. Le Goff A, Holzinger M, Cosnier S (2011) Enzymatic biosensors based on SWCNT-conducting polymer electrodes. Analyst 136:1279–1287
14. Wang J, Musameh M (2005) Carbon-nanotubes doped polypyrrole glucose biosensor. Anal Chim Acta 539:209–213
15. Gao M, Dai L, Wallace GG (2003) Biosensors based on aligned carbon nanotubes coated with inherently conducting polymers. Electroanalysis 15:1089–1094
16. Baur J, Le Goff A, Dementin S et al (2011) Three-dimensional carbon nanotube–polypyrrole–[NiFe] hydrogenase electrodes for the efficient electrocatalytic oxidation of H_2. Int J Hydrog Energy 36:12096–12101

17. Le Goff A, Cosnier S (2011) Photocurrent generation by MWCNTs functionalized with bis-cyclometallated Ir(III)- and trisbipyridyl ruthenium(II)- polypyrrole films. J Mater Chem 21:3910–3915
18. Le Goff A, Holzinger M, Cosnier S (2011) Characterization of multi-walled carbon nanotube electrodes functionalized by electropolymerized tris(pyrrole-ether bipyridine) ruthenium (II). Electrochim Acta 56:3633–3640
19. Bartlett PN, Baumberg JJ, Birkin PR et al (2002) Highly ordered macroporous gold and platinum films formed by electrochemical deposition through templates assembled from submicron diameter monodisperse polystyrene spheres. Chem Mater 14:2199–2208
20. Bartlett PN, Birkin PR, Ghanem MA (2000) Electrochemical deposition of macroporous platinum, palladium and cobalt films using polystyrene latex sphere templates. Chem Commun 1671–1672
21. Szamocki R, Reculusa S, Ravaine S et al (2006) Tailored mesostructuring and biofunctionalization of gold for increased electroactivity. Angew Chem Int Ed 45:1317–1321
22. Cernat A, Griveau S, Martin P et al (2012) Electrografted nanostructured platforms for click chemistry. Electrochem Commun 23:141–144
23. Santos L, Ghilane J, Lacroix J-C (2012) Surface patterning based on nanosphere lithography and electroreduction of in situ generated diazonium cation. Electrochem Commun 18:20–23
24. Sumida T, Wada Y, Kitamura T, Yanagida S (2000) Electrochemical preparation of macroporous polypyrrole films with regular arrays of interconnected spherical voids. Chem Commun 1613–1614
25. Tian S, Wang J, Jonas U, Knoll W (2005) Inverse opals of polyaniline and its copolymers prepared by electrochemical techniques. Chem Mater 17:5726–5730
26. Besombes J-L, Cosnier S, Labbé P (1996) Polyphenol oxidase-catechol: an electroenzymatic model system for characterizing the performance of matrices for biosensors. Talanta 43:1615–1619
27. Burestedt E, Narvaez A, Ruzgas T et al (1996) Rate-limiting steps of tyrosinase-modified electrodes for the detection of catechol. Anal Chem 68:1605–1611
28. Cosnier S, Mousty C, Gondran C, Lepellec A (2006) Entrapment of enzyme within organic and inorganic materials for biosensor applications: comparative study. Mater Sci Eng C 26:442–447
29. Wang S, Tan Y, Zhao D, Liu G (2008) Amperometric tyrosinase biosensor based on Fe3O4 nanoparticles–chitosan nanocomposite. Biosens Bioelectron 23:1781–1787
30. Dai Z, Xu X, Wu L, Ju H (2005) Detection of trace phenol based on mesoporous silica derived tyrosinase-peroxidase biosensor. Electroanalysis 17:1571–1577
31. Mousty C, Bergamasco J-L, Wessel R et al (2001) Elaboration and characterization of spatially controlled assemblies of complementary polyphenol oxidase–alkaline phosphatase activities on electrodes. Anal Chem 73:2890–2897
32. Cosnier S, Stoytcheva M, Senillou A et al (1999) A biotinylated conducting polypyrrole for the spatially controlled construction of an amperometric biosensor. Anal Chem 71:3692–3697
33. Zhang H, Meng Z, Wang Q, Zheng J (2011) A novel glucose biosensor based on direct electrochemistry of glucose oxidase incorporated in biomediated gold nanoparticles–carbon nanotubes composite film. Sensors Actuators B Chem 158:23–27
34. Hu F, Chen S, Wang C et al (2011) ZnO nanoparticle and multiwalled carbon nanotubes for glucose oxidase direct electron transfer and electrocatalytic activity investigation. J Mol Catal B Enzym 72:298–304
35. Jang HD, Kim SK, Chang H et al (2012) A glucose biosensor based on TiO_2–graphene composite. Biosens Bioelectron 38:184–188
36. Ryu J, Kim H, Lee S et al (2010) Carbon nanotube mat as mediatorless glucose sensor electrode. J Nanosci Nanotechnol 10:941–947